Electronic properties of straight, kinked, and branched Cu/Cu(111) quantum wires: A low-temperature scanning tunneling microscopy and spectroscopy study

Jérôme Lagoute, Xi Liu, and Stefan Fölsch
Paul-Drude-Institut für Festkörperelektronik, Hausvogteiplatz 5-7, D-10117 Berlin, Germany
(Received 10 February 2006; revised manuscript received 31 July 2006; published 11 September 2006)

Low-temperature scanning tunneling microscopy at 7 K is used to assemble monatomic native adatom chains on a Cu(111) surface and to study their *sp*-derived quantum states. The adatoms within the structure reside on equivalent nearest-neighbor lattice sites of the substrate surface (intrinsic Cu-Cu spacing 2.55 Å). Starting from linear chain segments, kinked chains and triple-terminal junctions are created, and the impact of the different structural details of the junction on the electronic properties is investigated by spectroscopic measurements. A simple tight-binding (TB) parametrization scheme is applied to discuss the experimentally observed energies and densities of the quantum states inherent to these chain structures of advanced complexity. The TB model also reveals potential overlaps of resonance-broadened states, which are not resolved in the experiment.

DOI: 10.1103/PhysRevB.74.125410 PACS number(s): 73.21.Hb, 73.22.−f, 68.37.Ef

I. INTRODUCTION

Apart from its central importance to device miniaturization, the controlled fabrication of surface-supported nanostructures opens up the possibility to create new material properties by confining electrons to dimensions where quantization phenomena are important. Low-temperature scanning tunneling microscopy (STM) and spectroscopy (STS) combine the capabilities of local probing and manipulating matter at the atomic level[1–3] and thus provide a powerful experimental technique to study the physics of perfect nanostructures serving as nanometric model systems. In the field of metal nanostructures, this approach was recently applied by Nilius *et al.*[4] to investigate confinement effects in monatomic Au chains assembled on a NiAl(110) surface. Their studies revealed the formation of unoccupied chain-confined quantum states[4,5] arising from the 6*s* states of the Au adatoms, which hybridize with the substrate states and develop p_z character.[6] These quantum states are localized in the pseudogap of the projected bulk bands of the NiAl(110) substrate.

In our subsequent studies, we showed that confined quantum states also exist in compact adatom structures of metallic one-component systems such as one-dimensional (1D) native adatom chains[7] and two-dimensional (2D) adatom islands[8] assembled on a Cu(111) surface. The latter study revealed that there is a natural linkage between the *sp* hybrid state associated with the discrete adatom,[9] the quantum states in assembled nanostructures, and the *sp*-derived Cu(111) Shockley surface state. In this sense, the quantum state formation in Cu/Cu(111) chains can be viewed as the 1D analogue of the traditional Shockley surface state existing at the extended surface. In the present work, we utilize Cu/Cu(111) adatom chains as a model system for quantum wire structures of advanced complexity: Linear monatomic chain segments are interconnected by means of atom manipulation to yield kinked and branched structures. The electronic properties of these objects are analyzed by spectroscopic measurements of the differential tunneling conductance, and they are discussed within a simple tight-binding parameterization scheme.

II. EXPERIMENTAL DETAILS

The experiments were carried out with an ultrahigh vacuum (UHV) STM operated at 7 K. A Cu(111) single crystal was cleaned in UHV by repeated Ne^+ sputtering cycles at 1 keV and subsequent annealing at 700 K. Chemically edged tungsten tips were used. Single Cu adatoms were created by controlled tip-surface contact at 7 K. In particular, the tunneling tip was dipped between 5 and 6 Å into the specimen surface and subsequently retracted to a final tip height of 6 Å while applying a voltage of −5 V to the tip-sample junction (the tunneling voltage refers to the sample with respect to the tip). By means of this procedure, discrete adatoms and clusters are created which are dispersed over the surface in the vicinity of the contact area. We find that only native adatoms are created in this way as indicated by the characteristic *sp*-derived Cu/Cu(111) adatom state located 3.3 eV above the Fermi level E_F.[7,9]

Single Cu adatoms can be manipulated at low temperature along arbitrary lateral directions at a tunneling resistance of ~0.1 MΩ by reducing the tip height to about 1.5 Å. These conditions are similar to the experimental parameters reported for the manipulation of Ag adatoms on Ag(111).[10] The values of tip height z quoted here and in the following refer to zero height at point contact between the STM tip and the specimen. Similar to experimental procedures reported previously,[10–13] the tip height was calibrated by current versus z measurements in which the event of contact was identified from the appearance of a discontinuity in the current accompanied by a contact conductance in the range of $2e^2/h$. Previous work[11–14] also showed that adhesive forces give rise to relaxation effects when the tip is in close proximity to the metal surface: Relaxations of tip and surface atoms lead to point contact at a reduced tip-sample distance which is smaller by roughly the typical atomic bond length as compared to the geometric tip-sample distance in the absence of relaxations.

Spectroscopic measurements of the differential tunneling conductance dI/dV were performed using a conventional lock-in technique (modulation amplitude and frequency:

30 mV at 600 to 700 Hz) to obtain information on the local density of states (LDOS).[15] Prior to these measurements, the STM tip was optimized by controlled tip-sample contact. The final tip condition was checked by spectroscopic reference measurements of inherent electronic surface features such as the Cu(111) surface state band onset[16] and a smooth variation of the local density of states within the pseudogap of the projected Cu bulk bands.[7]

III. RESULTS AND DISCUSSION

A. Tight-binding description of linear adatom chains

To analyze the confinement behavior of more complex Cu/Cu(111) quantum wire structures, we first consider that linear monatomic Cu/Cu(111) chains exhibit unoccupied quantum states giving rise to pronounced resonances in the differential tunneling conductance dI/dV within the pseudogap of the $\langle 111\rangle$-projected Cu bulk bands[7] [the pseudogap extends from about 1 eV below E_F to about 4.5 eV above E_F (Ref. 17)]. Density functional theory (DFT) calculations[9] showed that the chain-localized states derive from sp_z hybrid adatom states, which mix with substrate states. The sp_z state associated with the discrete Cu adatom is experimentally observed as a resonance at 3.3 eV above E_F with a half width of 0.6 eV. dI/dV mapping of the chain-localized states revealed LDOS oscillations along the chain indicative of quasi-one-dimensional quantum confinement. This observation is illustrated in Fig. 1(a) showing dI/dV signal profiles measured along a Cu_7 chain at tunneling voltages corresponding to the four lowest quantum state energies (see bold lines). Clearly, the state density distribution of the ground state with $n=1$ is characterized by a single lobe (see bottom curve) while n lobes are observed for the excited states of successive order n. The profiles corresponding to the excited states with $n=3$ and $n=4$ also indicate a marked enhancement of the end lobes. This characteristic enhancement is increasingly pronounced for higher excited states with shorter wavelength of the state density oscillation.[7] A similar behavior was previously observed experimentally for monatomic Au chains on NiAl(110).[4,5] Persson performed a computational study of electronic states in Au/NiAl(110) chains.[6] It was argued, on the basis of a TB analysis, that the LDOS enhancement at the chain ends is due to (i) the interference between the atomic wave functions of the chain atoms and (ii) the effect of overlapping LDOS distributions associated with the resonance-broadened states.

Figure 1(b) summarizes the experimental quantum state energies $E(n)$ [see circles, squares, triangles, and diamonds] of linear Cu/Cu(111) chains versus the number N of atoms within the chain. For short chains ($N \leqslant 7$), the energies were directly extracted from the resonance peaks in dI/dV point spectra measured at various positions of the assembled structure.[7] For longer chains with a decreased level spacing (i.e., an increased overlap of the resonance-broadened states), the bias-dependent evolution of the characteristic state density oscillations was evaluated to ensure an accurate energy determination. The profiles drawn as thin lines in Fig. 1(a) illustrate intermediate LDOS oscillations between consecutive eigenstates. Each set of symbols in Fig. 1(b) represents a specific quantum level in the regime of unoccupied states starting from the ground state with $n=1$ (empty circles) up to the excited state with $n=8$ (gray diamonds).

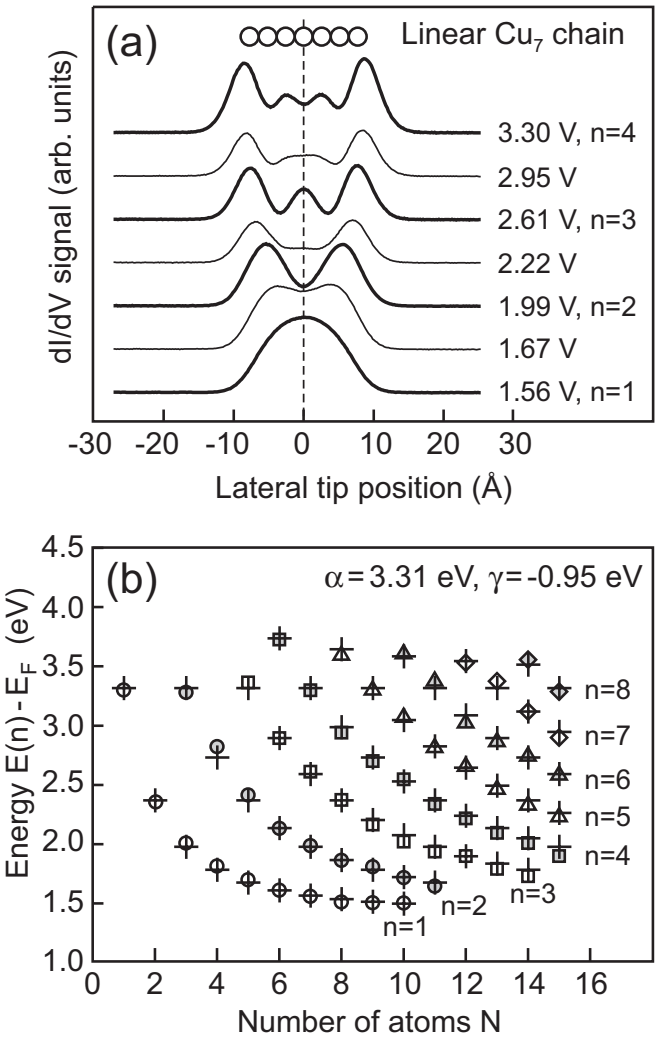

FIG. 1. (a) Experimental dI/dV signal profiles measured along a linear Cu_7 chain at the indicated tunneling voltages; bold lines show the state density oscillations of the four lowest quantum states starting from the ground state, $n=1$ (bottom curve) up to the excited state with $n=4$ (top curve), thin lines show LDOS oscillations between consecutive quantum states. (b) Experimental energies of the unoccupied quantum states vs the number N of atoms within the linear Cu/Cu(111) chains (data points are indicated by circles, squares, triangles, and diamonds); crosses mark the calculated eigenvalues of the tight-binding secular determinant with the binding energy $\alpha=3.31$ eV and the hopping integral $\gamma=-0.95$ eV and provide excellent agreement between calculation and experiment.

The observed eigenstate energies are described to an excellent degree by a simple tight-binding (TB) parametrization scheme. This is indicated by the crosses in Fig. 1(b), which mark the calculated eigenvalues $E(n)=\alpha+2\gamma\cos[n\pi/(N+1)]$ of the $N\times N$ TB secular determinant, implying a treatment of the atomic chain as an artificial linear molecule within the simple Hückel scheme.[18] In this parametrization, the quantity α is associated with the

binding energy of the atomic orbital, and all atoms are treated identically, meaning that all α values in the determinant are equal. The hopping integral γ, on the other hand, describes the overall coupling between adjacent orbitals arising from both direct interatomic coupling as well as substrate-induced coupling.[6] The present TB parameters thus include the effect of the supporting Cu(111) substrate, namely the specific binding energy of the atomic state interacting with the surface and the coupling between nearest neighbor chain atoms mediated by the substrate. The eigenvalues marked by crosses in Fig. 1(b) are obtained with the TB parameters α=3.31 eV and γ=−0.95 eV.[19] These values are consistent with (i) the resonance measured for the discrete adatom, and (ii) the position and width of the 1D energy band which we have previously derived by evaluating the dispersion of the chain-localized states.[7] Figure 1(b) illustrates that the TB model provides a good approximation to reproduce the experimental eigenstate energies over the entire range of chain length and quantum level order investigated. It is also noted at this point that earlier theoretical work[6,20] demonstrated that tight-binding modeling agrees with DFT calculations, revealing essential features of confinement and quantum size effects in surface-supported one-dimensional atomic metal chains.

B. Kinked and branched adatom chains

Kinked Cu chains were assembled by lateral manipulation of single Cu/Cu(111) adatoms under similar conditions used to construct simple Cu chains. The junctions of the structures are stabilized by a close-packed Cu trimer while the extremities correspond to monatomic Cu chains along the in-plane ⟨110⟩ directions with an included angle of 60°. Analogous to the case of linear Cu/Cu(111) chains,[21] the Cu atoms in kinked chains reside on adjacent face-centered cubic hollow sites of the substrate (Cu-Cu spacing 2.55 Å). Figure 2 shows a constant-current topograph obtained for a symmetric V-shaped Cu_{17} kink with three atoms included in the interconnecting compact trimer and seven atoms comprising each of the monatomic extremities oriented along the $[0\bar{1}1]$ and $[\bar{1}01]$ direction. The total length of the structure measured along either of the two extremities is 24.9 Å, which is very close to the measured length of a linear Cu_9 chain (24.6 Å). The constant-current STM images in Figs. 3(a)–3(c) show kinked chains of reduced size corresponding to a Cu_9 kink with three atoms along each extremity shown in Fig. 3(a), a Cu_{10} kink with three/four atoms within the left/right extremity shown in Fig. 3(b), and a Cu_{11} kink with four atoms each shown in Fig. 3(c). The electronic properties of these kinked Cu chains were probed by taking dI/dV spectra [Fig. 3(d)] with the tip located at the respective positions marked in the STM images. The measurements indicate the existence of discrete quantum levels for these structures of advanced complexity with eigenstate energies significantly different from those of linear chains containing the same number of atoms. In particular, for the symmetric Cu_9 kink [Fig. 3(d), top panel], three distinct peaks are observable at sample biases between zero and 4 V. Adding an atom to the right extremity yields an asymmetric Cu_{10} kink for which five

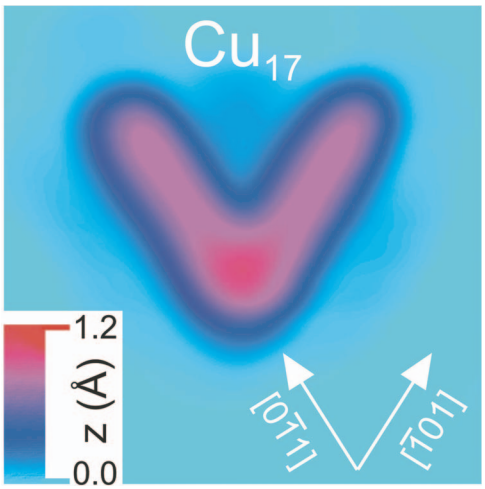

FIG. 2. (Color online) Constant-current STM image of a symmetric Cu_{17} kink (48 Å×48 Å surface area, 1 nA tunneling current, 60 mV sample bias) assembled on Cu(111) by atom manipulation at 7 K. The structure is comprised of a compact interconnecting Cu trimer and two monatomic extremities composed of seven atoms each, which are oriented along the $[0\bar{1}1]$ and $[\bar{1}01]$ directions, and separated by an angle of 60°. Cu atoms within the structure reside on nearest-neighbor surface lattice sites (Cu-Cu spacing 2.55 Å).

separate peaks are found (center panel) while three peaks are recovered for the symmetric Cu_{11} kink (bottom panel) obtained after incorporating a fourth atom into the left extremity. The steady increase in dI/dV signal at high sample bias, which is evident from the spectra shown in Fig. 3(d), is attributed to the extension of the pseudogap and the onset of image states below the vacuum level.[17]

To analyze this behavior in detail, we measured the spatial variation of the local density of states (LDOS) [see Figs. 4(a)–4(k)] by mapping the dI/dV signal at constant tip height and at bias voltages where peaks in the point spectra are observed. The data reveal that (i) the ground state density (characterized by the absence of a nodal plane) is predominantly localized at the interconnecting trimer [see Figs. 4(a), 4(d), and 4(i)] and that (ii) the ground state energy is lower as compared to linear chains with the same N (for the structures shown in Fig. 3, the lowering amounts to approximately 0.15 eV). This behavior is reasonable since the increased coordination due to the interconnecting trimer should reduce the energy of the system. For the asymmetric Cu_{10} kink, the dI/dV maps indicate an enhanced LDOS distribution on either one or the other extremity of the structure while the measured density distributions of the Cu_9 and the Cu_{11} kink are symmetric. This observation suggests that the dI/dV maps of the symmetric structures in Figs. 4(b), 4(c), 4(j), and 4(k) involve either degenerated states or overlapping states, which are not resolved in the measurement due to their intrinsic resonance broadening,[22] and a symmetric LDOS distribution.

The presence of overlapping resonance-broadened states is verified by calculating the five lowest eigenstates of a Cu_9 kink within the TB framework. The eigenvalues (yielding the quantum state energies) and the eigenvectors [yielding the

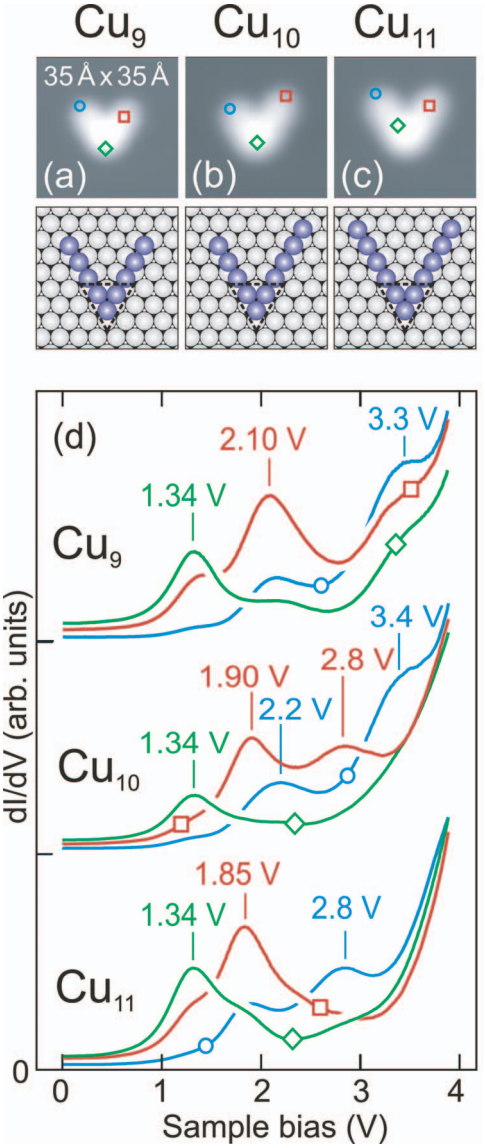

FIG. 3. (Color online) Top panel: Constant-current STM images (35 Å × 35 Å, 1 nA, 1 V) of a Cu_9 (a), a Cu_{10} (b), and a Cu_{11} kink (c) together with related sphere models of the structures (the compact trimer at the junction is indicated by the dashed black line). The dI/dV spectra in (d) were taken at lateral tip positions marked in the STM images (see circles, squares, and diamonds) and reveal pronounced resonance peaks in the differential tunneling conductance; five peaks are observed for the Cu_{10} kink while three peaks occur for the Cu_9 and the Cu_{11} kink (tunneling parameters before opening the feedback loop: 1 nA, 1 V).

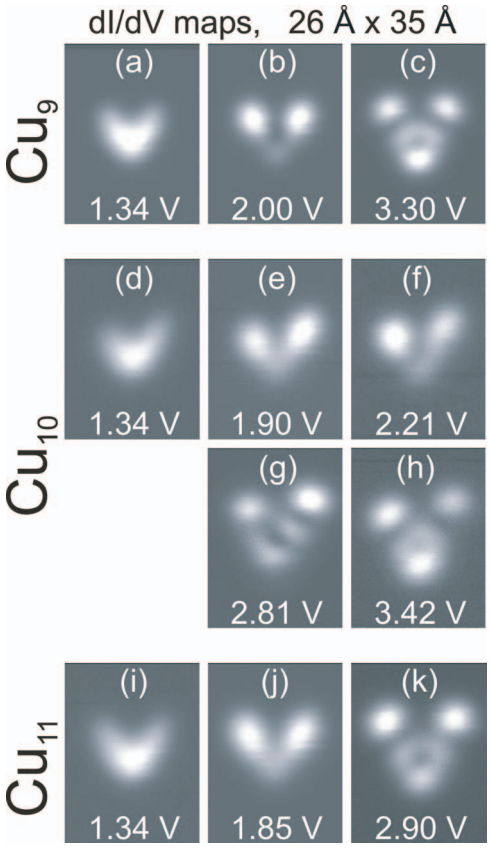

FIG. 4. (Color online) dI/dV maps (26 Å × 35 Å) of the kink structures shown in Figs. 3(a)–3(c) measured at constant tip height and at biases at which resonance peaks in the point spectra are observed [see Fig. 3(d)]; the dI/dV maps indicate characteristic LDOS variations of the Cu_9 (a)–(c), the Cu_{10} (d)–(h), and the Cu_{11} kink structure (i)–(k). Tunneling parameters before opening the feedback loop: 1 nA, 1 V.

coefficients for the linear combination of atomic orbitals (LCAO)] were numerically calculated from the secular determinant, and an *s*-like radial orbital character was assumed to approximate the decay of the atomic wave functions centered at the atomic sites within the structure. A realistic value of the decay constant was determined by measuring the resonance associated with the single adatom at 3.3 V sample bias as a function of the tip-to-surface separation ranging from 9 to 11 Å. As a result, an exponential decay in the dI/dV peak magnitude is found, which is characterized by a decay constant of 1.66 $Å^{-1}$. Since the differential tunneling conductance is a measure of the squared wave function, the decay constant describing the wave function vacuum tail was set to 0.83 $Å^{-1}$. The TB parameters were fixed to the values $\alpha=3.31$ eV and $\gamma=-0.95$ eV as obtained for the linear Cu adatom chains [Fig. 1(b)].

Figure 5 compares the measured dI/dV maps of the Cu_9 kink [Figs. 5(a)–5(c)] with grayscale plots of the squared wave function amplitude $|\Psi|^2$ of the five lowest states, see Figs. 5(d)–5(h). The $|\Psi|^2$ maps show the calculated state density distribution in a plane 8 Å above the topmost Cu atom layer of the surface. This choice of parameters is according to the experimental conditions during dI/dV mapping because (i) the initial tip height (relative to tip-surface contact) is about 5.5 Å (prior to opening the feedback loop at 1 nA and 1 V), and (ii) the formation of contact driven by tip-surface adhesion has to be taken into account by an increment on the order of the typical bond length (see also related discussion in Sec. II). The atomic positions within the structure are indicated by circles in Figs. 5(d)–5(h). The ground state is well reproduced with the wave-function amplitude predominantly localized at the trimer. The corresponding eigenstate energy is $E(1)=1.05$ eV, which is 290 meV below the measured ground state energy. The first

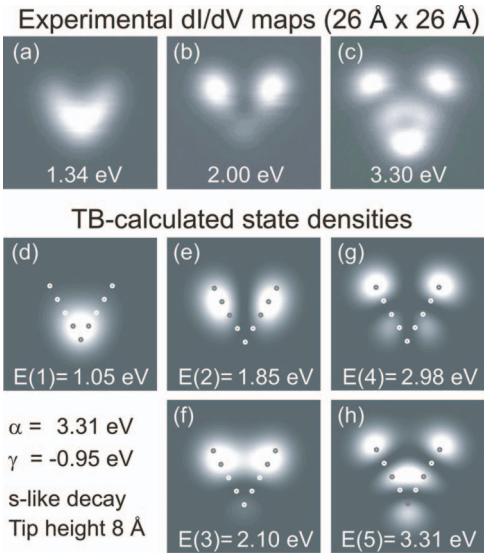

FIG. 5. (Color online) Experimental dI/dV maps (26 Å $\times$26 Å) obtained for the Cu_9 60° kink (a)–(c) and state density maps (d)–(h) corresponding to the squared wave function amplitudes of the five lowest eigenstates calculated within the TB scheme in a plane 8 Å above the topmost Cu atom surface layer (atomic positions within the kink are indicated by circles). While the dI/dV map in (a) is reproduced by the ground state in (d), the dI/dV maps in (b) and (c) are consistent with the superposition of two resonance-broadened states [(e) and (f) in correspondence to (b), and (g) and (h) in correspondence to (c)]. See discussion in the text for details on the calculation procedure.

and second excited states are found at $E(2)=1.85$ eV and $E(3)=2.10$ eV, respectively. These values are close to the second lowest peak of the spectra in Fig. 3(d) (top panel) and the corresponding experimental dI/dV map in Fig. 5(b). The first excited state [Fig. 5(e)] shows two lobes located on the linear extremities, and the second excited state [Fig. 5(f)] exhibits two lobes close to the ends of the extremities plus a third faint lobe at the junction. The third excited state [Fig. 5(g)] at $E(4)=2.98$ eV and the fourth excited state [Fig. 5(h)] at $E(5)=3.31$ eV are similar in energy to the right-hand side peak in the spectra of the Cu_9 kink and to the corresponding dI/dV map in Fig. 5(c). These results show that the resonances found at 2.10 V and ~3.3 V in the dI/dV spectra [see Fig. 3(d)] and the corresponding LDOS distributions in Figs. 5(b) and 5(c) involve two states each which are not experimentally resolved due to intrinsic level broadening. The present analysis, based on the TB parameters obtained for the linear chains, thus provides a straightforward, qualitative description of the observed dI/dV resonances and the corresponding LDOS distributions. However, there exists a systematic underestimation of the eigenstate energies—in particular, of the ground state energy. Similarly, we find that the ground state energy of the asymmetric Cu_{10} chain [see Fig. 3(b)] is underestimated by 300 meV while the excited state energies are ~170 meV below the experimental values (not shown).

Next, we address Y-shaped branched adatom chains in order to further increase the structural complexity. These structures constitute a model system for the study of interconnected atomic quantum wires. Starting with a Cu_9 kink as

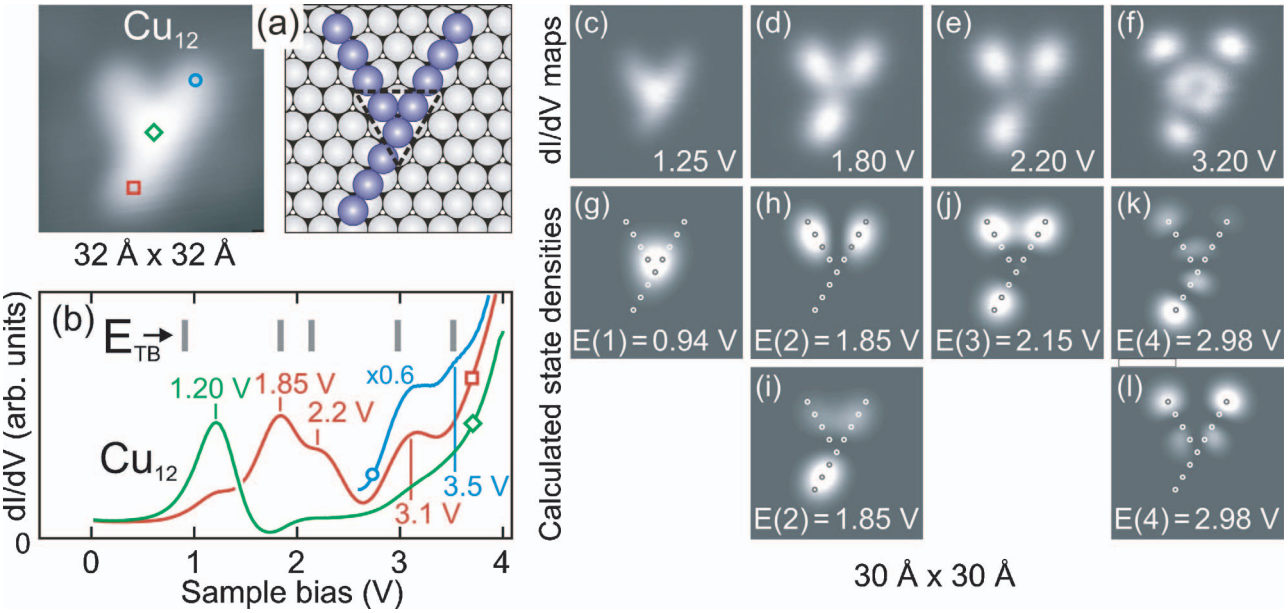

FIG. 6. (Color online) (a) Constant-current STM image (32 Å$\times$32 Å, 0.5 nA, 50 mV) of a Cu_{12} branched structure comprised of a compact Cu trimer at the junction and three Cu atoms in each of the three linear extremities along ⟨110⟩ (see right panel for corresponding sphere model). (b) dI/dV spectra taken at different locations of the structure indicating four resonance peaks plus a weak shoulder at ~3.5 V. The dI/dV maps in panels (c)–(f) relate to the four lowest resonances in the spectra in (b) and are well described by the state density maps in panels (g)–(l) calculated in a plane 8 Å above the topmost Cu atom surface layer. The analysis indicates degeneracy of the first excited state [(h) and (i) in correspondence to (d)] and of the third excited state [(k) and (l) in correspondence to (f)]. Vertical bars in (b) mark the TB-calculated energy values. Tunneling parameters prior to opening the feedback loop during the spectroscopic measurements: 1 nA tunneling current and 1 V sample bias.

shown in Fig. 3(a), a third monatomic extremity was added by attaching three additional atoms to the interconnecting trimer. The constant-current image of the resulting Cu_{12} branch in Fig. 6(a) reveals a Y-shaped structure consisting of a compact trimer at the junction and three extremities comprised of three atoms each (see related sphere model). dI/dV spectra were measured at different locations as indicated in the STM image. The spectrum taken at the center of the structure indicates a single peak at 1.20 V, see curve marked by a diamond in Fig. 6(b). By positioning the STM tip over the extremities, on the other hand, three additional peaks are found at 1.85 V, 2.2 V, and 3.1 V, as well as a shoulder at ~3.5 V (see curves marked by a circle and a square). The resonance at 1.20 V, which we attribute to the ground state, is again lower in energy as compared to the ground state of a Cu_{12} kink (1.35 eV) and the ground state of a linear Cu_{12} chain (~1.5 eV) comprised of the same number of atoms. The dI/dV maps corresponding to the observed peaks are shown in Figs. 6(c)–6(f). Clearly, the fundamental state is localized at the junction, which is consistent with the point spectrum taken in the center of the structure indicating a significant contribution of the peak at 1.20 V at this location. The first and second excited state, in Figs. 6(d) and 6(e) respectively, both exhibit three LDOS maxima with the lobes of the second excited state located closer to the ends of the extremities. Finally, the dI/dV map in Fig. 6(f) shows a LDOS maximum at each chain end and a circular feature around the center.

Figures 6(g)–6(l) show the TB-calculated $|\Psi|^2$ maps of the four lowest states of the Cu_{12} branch and the vertical bars in Fig. 6(b) summarize the TB-calculated eigenstate energies, indicating an appreciable underestimation for the ground state along with a reasonable agreement for the excited states. The calculation procedure is the same as described in connection with Fig. 5. The calculated state density of the fundamental state in Fig. 6(g) closely resembles the measured dI/dV map in Fig. 6(c) while the obtained ground state energy $E(1)=0.92$ V is 280 meV below the experimental value [i.e., similar in deviation as in the case of the kinked structures, see Figs. 5(a) and 5(d)]. The first excited state found at $E(2)=1.85$ V is in agreement with the experimentally observed energy and appears to be doubly degenerate within the TB model,[23] see the $|\Psi|^2$ maps in Figs. 6(h) and 6(i). The corresponding experimental dI/dV map in Fig. 6(d) is well described by a superposition of these two degenerate states. Similarly, twofold degeneracy is also found for the TB-calculated third excited state as apparent from the $|\Psi|^2$ maps in Figs. 6(k) and 6(l), and the total density of this state is consistent with the measured dI/dV map in Fig. 6(f).

For the second excited state at 2.15 V, the TB analysis indicates a major wave-function amplitude contribution associated with the two outermost atoms of the extremities (the LCAO coefficients are 0.327 and 0.399 for the outmost atom and its nearest neighbor, respectively), while a minor contribution results from the atoms of the interconnecting trimer (characterized by a coefficient of 0.204 for each trimer atom). The corresponding center lobe is very weak in the $|\Psi|^2$ map in Fig. 6(j) calculated at 8 Å above the surface (to match with the experimental conditions) while it becomes clearly visible when calculating the $|\Psi|^2$ map at a reduced

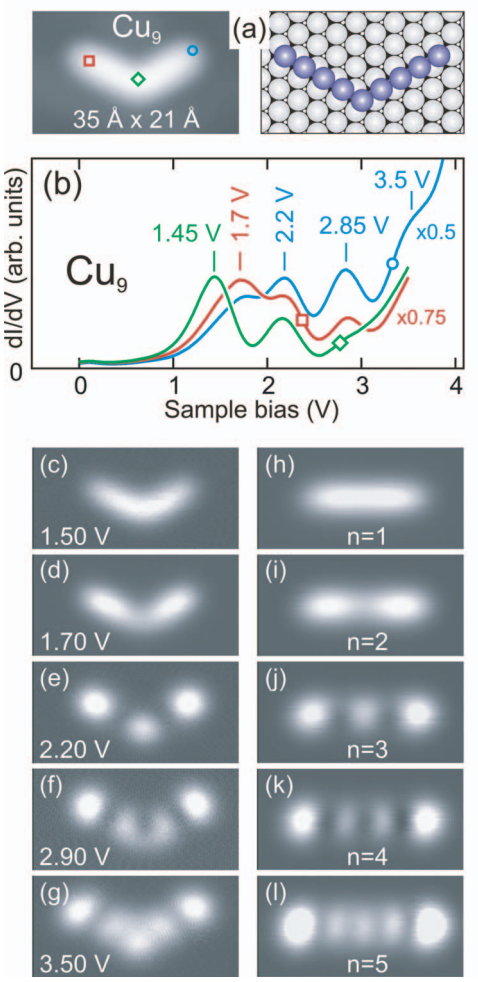

FIG. 7. (Color online) (a) Constant-current STM image (35 Å ×21 Å, 1 nA, 80 mV) of a symmetric Cu_9 chevron with an included angle of 120° and corresponding sphere model. (b) dI/dV spectra taken at different locations of the structure indicating four resonance peaks and a weak shoulder at ~3.5 V. The corresponding dI/dV maps of the chevron in panels (c)–(g) are similar to the dI/dV maps obtained for a straight Cu_9 chain [see panels (h)–(l)] in terms of the eigenstate energies and the number of lobes and nodes of the squared wave functions. Tunneling parameters prior to opening the feedback loop during the spectroscopic measurements: 1 nA tunneling current and 1 V sample bias.

height of, e.g. 4 Å (not shown). Accordingly, three pronounced lobes at the extremities are observed experimentally [see Fig. 6(e)], and the dI/dV spectrum taken in the center of the structure [see curve marked by a diamond in Fig. 6(b)] shows only a weak shoulder slightly above 2 V. Note also that the position and shape of the three lobes measured at 2.20 V [Fig. 6(e)] as compared to those at 1.80 V [Fig. 6(d)] is consistent with the calculation in which the lobes cover three atomic sites at 1.85 V [Figs. 6(h) and 6(i)] but only two atomic sites at 2.15 V [Fig. 6(j)].

Aside from kinked and branched adatom chains involving a compact trimer as the interconnecting building block of the structure, we also studied chains with intrinsic defects leading to a break in symmetry but without a change in the number of nearest neighbors. Such a structure is shown in Fig. 7(a) which corresponds to a kinked Cu_9 chain with mon-

atomic extremities of equal length and an included angle of 120°. Assembly of such kinked chains by STM-based atom manipulation is more delicate as compared to the assembly of 60° kinks stabilized by a compact trimer. Furthermore, they are more sensitive to tip-induced degradation. The dI/dV point spectra in Fig. 7(b) indicate five resonances with the ground state peak centered at 1.45 V. Because of resonance broadening, we observe an overlap of the peaks corresponding to the excited states which are nevertheless clearly distinguished. The peaks are located at 1.7 V, 2.2 V, and 2.85 V, together with a faint shoulder at ~3.5 V. The corresponding eigenstate energies are close to those determined for the linear Cu_9 chain, namely 1.51 eV for the ground state and 1.81 eV, 2.17 eV, 2.70 eV, and ~3.3 eV for the excited states. The bottom panel of Fig. 7 shows related dI/dV maps of the Cu_9 chevron [Figs. 7(c)–7(g), left column] and the linear Cu_9 chain [Figs. 7(h)–7(l), right column] taken at bias voltages close to the respective eigenstate energies. We find a clear correspondence between the two sets of state densities concerning the number of lobes and nodal planes of the squared wave functions. Note that the LDOS between the two lobes in Figs. 7(d) and 7(i) is nonzero because the resonance broadening leads to a nonnegligible contribution of the ground state at the energy of the first excited state. Comparing the results discussed in connection with Figs. 5 and 6, deviations from the TB model (which reproduces the eigenstate energies of linear Cu chains on a quantitative level) are predominantly due to a changed atomic coordination within the junction (such as for kinks with an included angle of 60°) rather than a break in symmetry (such as for chevrons with an included angle of 120°).

IV. CONCLUSIONS

This work demonstrates that the STM-based assembly of Cu/Cu(111) model quantum wires by atom manipulation is not restricted to the creation of linear adatom chains; it also allows one to build more complex structures such as kinked and branched chains with different symmetries and different structural details of the interconnecting junction. We find that the electronic states in these atomic-scale structures are well described by a TB model which takes into account nearest-neighbor interactions among the adatoms and includes only one atomic orbital along with identical TB parameters for every atom.

While the eigenstate energies of linear chains are reproduced to an excellent degree, a systematic underestimation is found for chain structures involving junctions with an increased coordination of the atoms (i.e., the kinked and branched wires discussed in connection with Figs. 3 and 6). The deviation is largest for the ground state which is predominantly localized at the junction of the structures. This departure from quantitative agreement is not surprising considering the fact that the physics of all relevant interactions is parameterized in a very simple form. We find best agreement with the TB model for structures with uniform symmetry such as linear monatomic chains or compact triangular adatom islands as reported previously.[8] The observation that the TB parameters describing the latter two cases are different [$\alpha=3.31$ eV and $\gamma=-0.95$ eV for linear Cu/Cu(111) chains, $\alpha\cong 3.8$ eV and $\gamma\cong -0.7$ eV for triangular Cu/Cu(111) islands[8]] reflects the fact that the overall interactions amongst the adatoms and the substrate strongly depend on the symmetry and local environment within the structure (indicating strong interatomic wave function coupling). For structures with mixed symmetry, such as kinked chains with monatomic extremities joined by a compact trimer, a systematic improvement in agreement is not achievable by changing the α and γ parameters of highly coordinated adatoms to the values found in the analysis of compact Cu/Cu(111) islands (or to any other set of optimized values). Apparently, such an additive approach within the TB parametrization does not fully reproduce all effects of local environment and coordination—which is, after all, not surprising regarding the simplicity of the model. Future theoretical investigations using more elaborate calculation techniques such as DFT are highly desirable in order to gain fundamental insight into how atomic-scale structure determines wave function coupling and adstructure-substrate interaction. Nonetheless, it is pointed out that the TB parametrization scheme employed here is instructive and straightforward in describing the evolvement of quantum confinement when building model structures in an atom-by-atom fashion. The present results show that the TB model reproduces major features of the confinement in assembled adatom structures of advanced complexity. This approach verifies the energies and the squared wave functions of the quantum states, and it reveals overlaps due to resonance broadening of the states which are not resolved in the experiment.

The present study does not indicate any appreciable edge effects in the sense of altered electronic states associated with the atoms at the end of the Cu/Cu(111) chain structures. In contrast, such changes were recently reported for self-assembled Au adatom chains on Si(553) (Ref. 24) exhibiting individual end states with a substantial energy shift from the unoccupied to the occupied states. We speculate that this difference in behavior is due to inherent structural differences between the two systems: While in the present metallic one-component system the chain atoms reside on equivalent nearest-neighbor lattice sites of the Cu(111) surface,[21] Au-induced reconstruction of the covalent Si(553) surface involves structural elements such as the rebonding of Si atoms and substitutional Au adsorption leading to the formation of 1D Au adatom chain structures.[25,26]

ACKNOWLEDGMENTS

The authors thank Jascha Repp, Gerhard Meyer, Per Hyldgaard, Fredrik E. Olsson, and Mats Persson for inspiring discussions and James A. H. Stotz for a critical reading of the manuscript. This research was financially supported by the European Union (RTN network project NANOSPECTRA, Contract No. RTN2-2001-00311).

[1] D. M. Eigler and E. K. Schweizer, Nature **344**, 524 (1990).
[2] J. A. Stroscio and D. M. Eigler, Science **254**, 1319 (1991).
[3] G. Meyer, S. Zöphel, and. K. H. Rieder, Phys. Rev. Lett. **77**, 2113 (1996).
[4] N. Nilius, T. M. Wallis, and W. Ho, Science **297**, 1853 (2002).
[5] T. M. Wallis, N. Nilius, and W. Ho, Phys. Rev. Lett. **89**, 236802 (2002).
[6] M. Persson, Phys. Rev. B **70**, 205420 (2004).
[7] S. Fölsch, P. Hyldgaard, R. Koch, and K. H. Ploog, Phys. Rev. Lett. **92**, 056803 (2004).
[8] J. Lagoute, X. Liu, and S. Fölsch, Phys. Rev. Lett. **95**, 136801 (2005).
[9] F. E. Olsson, M. Persson, A. G. Borisov, J.-P. Gauyacq, J. Lagoute, and S. Fölsch, Phys. Rev. Lett. **93**, 206803 (2004).
[10] S.-W. Hla, K.-F. Braun, and K.-H. Rieder, Phys. Rev. B **67**, 201402(R) (2003).
[11] U. Dürig, O. Züger, and D. W. Pohl, Phys. Rev. Lett. **65**, 349 (1990).
[12] L. Limot, J. Kröger, R. Berndt, A. Garcia-Lekue, and W. A. Hofer, Phys. Rev. Lett. **94**, 126102 (2005).
[13] L. Olesen, M. Brandbyge, M. R. Sørensen, K. W. Jacobsen, E. Lægsgaard, I. Stensgaard, and F. Besenbacher, Phys. Rev. Lett. **76**, 1485 (1996).
[14] W. A. Hofer, A. J. Fisher, R. A. Wolkow, and P. Grütter, Phys. Rev. Lett. **87**, 236104 (2001).
[15] R. M. Feenstra, Surf. Sci. **299/300**, 965 (1994).
[16] M. F. Crommie, C. P. Lutz, and D. M. Eigler, Nature (London) **363**, 524 (1993).
[17] N. V. Smith, Phys. Rev. B **32**, 3549 (1985).
[18] P. Atkins and J. de Paula, *Physical Chemistry* (Oxford University Press, Oxford, 2005).
[19] The binding energy α is measured relative to the Fermi level. Different from our previous definition of sign used in Refs. 7 and 8, the hopping integral γ is defined as a negative quantity in the case of an *s*-like energy band dispersion.
[20] F. Liu, S. N. Khanna, and P. Jena, Phys. Rev. B **42**, 976 (1990).
[21] J. Repp, G. Meyer, K. H. Rieder, and P. Hyldgaard, Phys. Rev. Lett. **91**, 206102 (2003).
[22] From dI/dV point spectra, a half width of about 0.6 eV is estimated, which is in the range of the broadening observed for linear chains.
[23] The TB model only takes into account the coordination of identical atomic building blocks and assumes identical nearest-neighbor coupling so that true degeneracy may be lifted due to the detailed symmetry of the structure as well as site-specific substrate-mediated coupling.
[24] J. N. Crain and D. T. Pierce, Science **307**, 703 (2005).
[25] J. N. Crain, J. L. McChesney, F. Zheng, M. C. Gallagher, P. C. Snijders, M. Bissen, C. Gundelach, S. C. Erwin, and F. J. Himpsel, Phys. Rev. B **69**, 125401 (2004).
[26] S. Riikonen and D. Sánchez-Portal, Nanotechnology **16**, S218 (2005).